Crystal Chemistry of Perovskite-Type Hydride $NaMgH_3$: Implications for Hydrogen Storage

Hui Wu,*[,†,‡] Wei Zhou,[†,‡] Terrence J. Udovic,[†] John J. Rush,[†,‡] and Taner Yildirim[†,§]

NIST Center for Neutron Research, National Institute of Standards and Technology, 100 Bureau Drive, MS 6102, Gaithersburg, Maryland 20899-6102, Department of Materials Science and Engineering, University of Maryland, College Park, Maryland 20742-2115, and Department of Materials Science and Engineering, University of Pennsylvania, 3231 Walnut Street, Philadelphia, Pennsylvania 19104-6272

Received November 26, 2007. Revised Manuscript Received January 11, 2008

The crystal structure, lattice dynamics, and local metal-hydrogen bonding of the perovskite hydride $NaMgH_3$ were investigated using combined neutron powder diffraction, neutron vibrational spectroscopy, and first-principles calculations. $NaMgH_3$ crystallizes in the orthorhombic $GdFeO_3$-type perovskite structure (*Pnma*) with $a^-b^+a^-$ octahedral tilting in the temperature range of 4 to 370 K. In contrast with previous structure studies, the refined Mg−H lengths and H−Mg−H angles indicate that the MgH_6 octahedra maintain a near ideal configuration, which is corroborated by bond valence methods and our DFT calculations, and is consistent with perovskite oxides with similar tolerance factor values. The temperature dependences of the lattice distortion, octahedral tilting angle, and atomic displacement of H are also consistent with the recently observed high H mobility at elevated temperature. The stability and dynamics of $NaMgH_3$ are discussed and rationalized in terms of the details of our observed perovskite structure. Further experiments reveal that its perovskite crystal structure and associated rapid hydrogen motion can be used to improve the slow hydrogenation kinetics of some strongly bound light-metal-hydride systems such as MgH_2 and possibly to design new alloy hydrides with desirable hydrogen-storage properties.

Introduction

The use of hydrogen as a primary fuel in the long term would greatly reduce CO_2 emissions and pollutants, as well as our dependence on the world's diminishing oil supplies. One of the major challenges in the quest to develop hydrogen-fueled vehicles is the development of lightweight materials that will absorb and release hydrogen in the range of 1–10 bar and 298–473 K.[1] Much effort has been focused on light-metal hydrides such as LiH and MgH_2 because of their relatively high hydrogen densities (>5 wt %). However, most of them have rather slow absorption kinetics, relatively high thermal stability, and/or problems with the reversibility of hydrogen absorption/desorption cycling. Recently, alloying with Si or Ge has been shown to destabilize these hydrogen-rich, yet strongly bound, light-metal hydrides at significantly lower temperatures.[2,3] Nonetheless, important challenges remain in improving their absorption kinetics and cycling capability. Investigations have also been made to enhance the storage properties of known complex hydrides[4–7] as well as to develop new complex hydrides containing main group III and V elements with high hydrogen capacities.[8,9] Unfortunately, most of these hydrides show poor kinetics and irreversibility with respect to hydrogen absorption/desorption, and suffer from the potential for toxic gas release (e.g., ammonia, diborane) during dehydrogenation. Nonetheless, ternary complex hydrides containing only alkali and/or alkaline-earth metals may enhance kinetics and reversibility and inhibit toxic-gas side products compared with the parent borohydride, amide (imide) and Alanate compounds.

Unlike the well-studied binary alkali and/or alkaline-earth metal hydrides, structural information available for ternary or even quaternary hydrides is considerably less owing to the complexity of their structural arrangements and difficulties involved in determining hydrogen positions by conventional X-ray diffraction (XRD) methods. Several attempts were made to prepare ternary hydrides with the formula $A_xAE_yH_{x+2y}$ (A = Na, K, Rb, Cs, AE = Mg, Ca),[10–13]

* To whom all correspondence should be addressed. Email: huiwu@nist.gov.
† National Institute of Standards and Technology.
‡ University of Maryland.
§ University of Pennsylvania.

(1) http://www.eere.energy.gov/.
(2) Vajo, J. J.; Mertens, F.; Ahn, C. C., Jr.; Fultz, B. *J. Phys. Chem. B* **2004**, *108*, 13977–13983.
(3) Wu, H.; Zhou, W.; Udovic, T. J.; Rush, J. J. *Chem. Mater.* **2007**, *19*, 329–334.
(4) Bogdanovic, B.; Schwickardi, M. *J. Alloys. Compd.* **1997**, *253*·*254*, 1–9.
(5) Lu, J.; Fang, Z. Z. *J. Phys. Chem. B* **2005**, *109*, 20830–20834.
(6) Luo, W.; Sickafoose, S. *J. Alloys Compd.* **2006**, *407*, 274–281.
(7) Xiong, Z.; Wu, G.; Hu, J.; Liu, Y.; Chen, P.; Luo, W.; Wang, J. *Adv. Funct. Mater.* **2007**, *17*, 1137–1142.
(8) Cerny, R.; Filinchuk, Y.; Hagemann, H.; Yvon, K. *Angew. Chem., Int. Ed.* **2007**, *46*, 5765–5767.
(9) Filinchuk, Y. E.; Yvon, K.; Meisner, G. P.; Pinkerton, F. E.; Balogh, M. *Inorg. Chem.* **2006**, *45*, 1433–1435.
(10) Ronnebro, E.; Noreus, D.; Kadir, K.; Reiser, A.; Bogdanovic, B. *J. Alloys Compd.* **2000**, *299*, 101–106.
(11) (a) Bouamrane, A.; Laval, J. P.; Soulie, J. -P.; Bastide, J. P. *Mater. Res. Bull.* **2000**, *35*, 545–547. (b) Park, H. -H.; Pezat, M.; Darriet, B.; Hagenmuller, P. *Rev. Chim. Miner.* **1987**, *24*, 525. (c) Maeland, A. J.; Lahar.; W, D. *Z. Phys. Chem.* **1993**, *179*, 181.
(12) Gingl, F.; Vogt, T.; Akiba, E.; Yvon, K. *J. Alloys Compd.* **1999**, *282*, 125.

10.1021/cm703356v CCC: $40.75
Published on Web 02/16/2008

$AE_xA_yH_{2x+y}$ (AE = Sr, Ba, A = Li),[14,15] and $AE'_xAE''_yH_{2(x+y)}$ (AE = Mg, Sr, and Ba).[13,16] Some of these are able to form a unique type of crystal structure---ABX_3 perovskite with a large *A* cation surrounded by 12 *X* anions and a small *B* cation coordinated with 6 *X* anions. It is well-known that ABO_3 perovskites constitute one of the most important and widely studied families of oxide compounds thanks to their interesting dielectric/ferroelectric properties, magnetic behavior, electronic and ionic conductivity, and superconductivity. Their flexibility in accommodating a broad range of atomic substitutions provides a robust platform for probing correlations between their varied properties and the underlying structural chemistry.[17]

Generally, ABX_3 perovskites can be described in terms of the close packing of the AX_3 layers, with B-site cations in the centers of the BX_6 octahedra. When the AX_3 layers are arranged via cubic close packing, the BX_6 octahedra are connected exclusively through corner sharing, and the structure is termed "cubic" perovskite. The deviation from the perfect cubic perovskite structure can be evaluated by the Goldschmidt tolerance factor ($t = (r_A + r_X) / \sqrt{2}(r_B + r_X)$). In an "ideal" cubic perovskite, the A and B cations realize their equilibrium bond distances to the X anions without inducing any distortion of the unit cell and $d_{A-X}=\sqrt{2}(d_{B-X})$. The resultant symmetry is cubic with space group *Pm-3m*, and $t = 1$. In many perovskites, the A−X and B−X bond lengths are geometrically incompatible, and the symmetry will be lowered. When the A cation is small ("undersized"), $t < 1$. The A−X length can be shortened and the coordination number of the *A* cation lowered through a correlated tilting of the surrounding BX_6 octahedra. Beginning with the pioneering studies of Glazer[18] and more recently by Woodward,[19] the variations in symmetry resulting from different types of octahedral tilting have been systematized and rationalized for simple and complex perovskites. When $t > 1$, the AX_3 layers typically adopt mixed cubic (*c*) and hexagonal (*h*), or pure hexagonal close packed stacking sequences. The resultant structure is called a "hexagonal" perovskite. The introduction of hexagonal stacking is accompanied by face-sharing of the adjacent BX_6 octahedra and by the formation of 90° B−X−B bond angles. In contrast to many examples of hexagonal perovskite oxides with differently mixed (*c*) and (*h*) layers, the only two examples of hexagonal perovskite hydrides are six-layer $(hcc)_2$ $RbMgH_3$ ($t = 1.041$, 6H-$BaTiO_3$-type)[12] and the high-pressure polymorph nine-layer $(chh)_3$ $CsMgH_3$ ($t = 1.093$, $BaRuO_3$-type).[20]

For perovskite hydrides, available crystallographic information is limited, with only eight reported perovskite-forming systems, i.e., $LiSrH_3$,[15] $LiBaH_3$,[15] $NaMgH_3$.[10] $KMgH_3$,[11] $RbMgH_3$,[12] $CsMgH_3$,[20] $RbCaH_3$,[11] and $CsCaH_3$.[12] No neutron diffraction data are available for $KMgH_3$, $RbCaH_3$, $LiSrH_3$, and $LiBaH_3$, which were assigned a *Pm-3m* perovskite structure from XRD results, and the hydrogen sites were restrained by the symmetry operation. Some of the reported structures are inconsistent with the general criteria for a stable perovskite structure because their tolerance factors were too small to maintain a cubic perovskite structure with *Pm-3m* symmetry. Some refined structures are questionable due to the unusually large distorted BX_6 octahedra which make the structure strained and crystallographically unstable. Furthermore, few studies have been done concerning their properties and applications. Because of the rich and well-established crystal chemistry of perovskites, we believe it is important to clarify and determine the structures of perovskite hydrides and rationalize their properties. Recently, researchers reported reversible hydrogenation/dehydrogenation with a 6 wt % hydrogen capacity in the perovskite hydride $NaMgH_3$.[21] Moreover, a rapid hopping motion of H has been observed in $NaMgH_3$ by NMR,[22] much faster than in MgH_2. It is clear that more structural details for $NaMgH_3$ are needed to determine if there is some correlation between this high hydrogen mobility and hydrogenation/dehydrogenation reversibility. Hence, in the present paper, we have investigated the crystal structure, lattice dynamics, and local metal-hydrogen bonding configuration of $NaMgH_3$, using combined neutron powder diffraction (NPD), neutron vibrational spectroscopy (NVS), and first-principles calculations. We have also studied the hydrogen-storage properties and dynamical behavior of $NaMgH_3$, as well as its potential to improve the hydrogenation thermodynamics and kinetics of other hydride systems.

Experimental Section

$NaMgH_3$ was prepared using standard solid-state methods. Stoichiometric quantities (1:1 ratio) of the binary hydrides, NaH (Aldrich,[23] 95%) and MgH_2(Alfa Aesar, 98%) were mixed via ball milling with a Fritsch Pulverisette 7 planetary mill at 400 rpm for 60 min. The powder mixture was then wrapped in a Mo envelope and sealed in a stainless steel tube. The tube was connected to a hydrogen gas tank, as a part of a hydrogenation system, and heated in a tube furnace. The powder mixture was heated overnight up to 623 K under 70 bar H_2 pressure. All sample handling was performed in a He-filled glovebox due to the extreme air-sensitivity of the

(13) Yvon, K.; Bertheville, B. *J. Alloys Compd.* **2006**, *425*, 101–108, and the references therein.
(14) Maeland, A. J.; Andresen, A. F. *J. Chem. Phys.* **1968**, *48*, 4660.
(15) Messer, C. E.; Eastman, J. C.; Mers, R. G.; Maeland, A. J. *Inorg. Chem.* **1964**, *3*, 776–778.
(16) (a) Gingl, F.; Yvon, K.; Fischer, P. *J. Alloys Compd.* **1994**, *206*, 73. (b) Gingl, F.; Hewat, A.; Yvon, K. *J. Alloys Compd.* **1997**, *253–254*, 17. (c) Gingl, F.; Yvon, K.; Vogt, T. *J. Alloys Compd.* **1997**, *256*, 155. (d) Gingl, F.; Bonhomme, F.; Yvon, K.; Fischer, P. *J. Alloys Compd.* **1992**, *185*, 273. (e) Bertheville, B.; Yvon, K. *J. Alloys Compd.* **1999**, *288*, 197.
(17) Davies, P. K.; Wu, H.; Borisevich, A. Y.; Molodetsky, I. E.; Farber, L., *Annu. Rev. Mater. Sci.* **2008**, submitted.
(18) Glazer, A. M. *Acta Crystallogr., Sect. B* **1972**, *28*, 3384–3392.
(19) (a) Woodward, P. M. *Acta Crystallogr., Sect. B* **1997**, *53*, 32–43. (b) Woodward, P. M. *Acta Crystallogr., Sect. B* **1997**, *53*, 44–66.
(20) Bertheville, B.; Fischer, P.; Yvon, K. *J. Alloys Compd.* **2002**, *330–332*, 152.
(21) (a) Ikeda, K.; Kogure, Y.; Nakamori, Y.; Orimo, S. *Scr. Mater.* **2005**, *53*, 319–322. (b) Ikeda, K.; Kato, S.; Shinzato, Y.; Okuda, N.; Nakamori, Y.; Kitano, A.; Yukawa, H.; Morinaga, M.; Orimo, S. *J. Alloys Compd.* **2007**, *446–447*, 162–165.
(22) Conradi, M.; Corey, B.; Bowman, Jr., R.; Zidan, R.; Stowe, A.,private communication.
(23) Certain commercial suppliers are identified in this paper to foster understanding. Such identification does not imply recommendation or endorsement by the NIST nor does it imply that the materials or equipment identified are necessarily the best available for the purpose.

hydrides. Phase identification and equilibrium were monitored on samples sealed in glass capillaries using a Rigaku diffractometer with a Cu Kα source operated at 40 kV and 40 mA.

All neutron scattering measurements were performed at the NIST Center for Neutron Research (NCNR). Neutron powder diffraction studies were conducted on the high-resolution neutron powder diffractometer (BT-1) with the Cu(311) monochromator at a wavelength of 1.5403(2) Å and an in-pile collimation of 15 min of arc. Data were collected over the 2θ range of 3–168°. Rietveld structural refinements were done using the GSAS package.[24] Because of the large incoherent neutron scattering cross section of hydrogen, the sample utilized in the NPD measurements was deuterated by exposing it to gaseous deuterium at a pressure of 50 bar and a temperature of 623 K over a 2 week period with several cycles of intermediate flushing and recharging of deuterium gas. The exchanged deuterium content was determined by gravimetric measurements, and the residual hydrogen content was checked using the neutron prompt-γ activation analysis (PGAA) facility, which is able to detect hydrogen as low as 2 μg.[25] Pure NaH and MgH_2 samples were used as standards to normalize γ-ray intensities. The final stoichiometry of H in the NPD sample was found to be Na: Mg:H = 1:1: 0.047.

Neutron vibrational spectra were measured at 5 K using the BT-4 Filter-Analyzer Neutron Spectrometer (FANS)[26] with the Cu(220) monochromator under conditions that provided energy resolutions of 2–4.5% over the vibrational energy range probed. First-principles calculations were performed within the plane-wave implementation of the generalized gradient approximation to density functional theory (DFT) using the PWscf package.[27] We used a Vanderbilt-type ultrasoft potential with Perdew-Burke-Ernzerhof exchange correlation. A cutoff energy of 408 eV and a 2 × 3 × 2 k-point mesh were found to be enough for the total energy and force to converge within 0.5 meV/atom and 0.005 eV/Å. Structure optimizations were performed with respect to lattice parameters and atomic positions. The phonon calculations were conducted with the optimized structure using the supercell method with finite difference. [28,29]

Results

1. Crystal Structure, Coordination, and Bonding. Indexing of XRD data of $NaMgH_3$ was consistent with the $GdFeO_3$-type perovskite structure with space group *Pnma*. The structure of $NaMgD_3$ was refined using NPD data at 5, 300, and 370 K. No phase transition was observed over the studied temperature range. Rietveld refinements were performed using the lattice parameters refined from X-ray powder diffraction data and the fractional coordinates with a $GdFeO_3$-type perovskite model. No cation site (Na/Mg) disordering was ascertained from the refinement, and thus the site occupancies of the Na and Mg atoms were fixed according to the chemical composition. The NPD pattern of $NaMgD_3$ at room temperature is shown in Figure 1 with

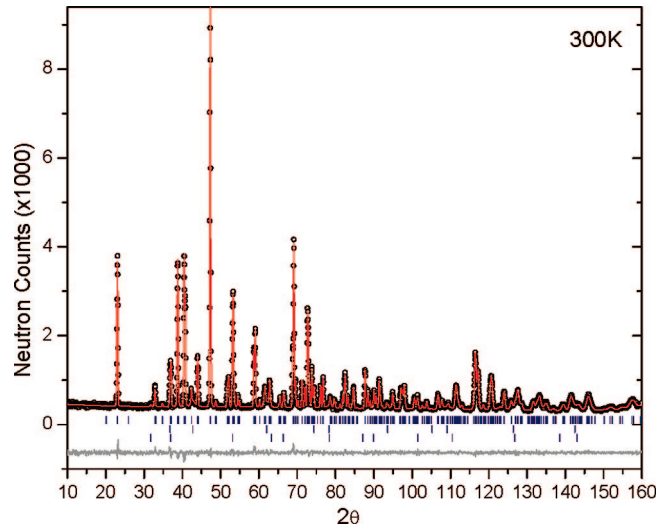

Figure 1. Experimental (circles), calculated (line), and difference (line below observed and calculated patterns) NPD profiles for $NaMgD_3$ at 300 K. Vertical bars indicate the calculated positions of Bragg peaks for $NaMgD_3$, MgO, and NaD (from the top), respectively.

excellent quality of the fit (see the Supporting Information for NPD patterns at 5 and 370 K). The refined lattice parameters, fractional coordinates, site occupancies, thermal parameters, and reliability factors for $NaMgD_3$ measured at 5, 300, and 370 K are summarized in Tables 1 and 2. Table 2 also compares the refined and calculated fractional coordinates in the present study with the previously reported values. The optimized structure from our DFT calculations is in good agreement with the refined structure in this work, but shows significant discrepancies with the earlier studies.

Consistent with the ABX_3 perovskite structure, each Na (A-site) cation is surrounded by 12 D anions, and each Mg (B-site) cation is coordinated with 6 D anions. Therefore, each D anion is bonded with 2 Mg and 4 Na cations. Selected interatomic bond distances and angles are given in Table 3. The Mg−D bond lengths are in the range of 1.9604(1)−1.9632(1) Å (300 K), longer than those in MgD_2.[30] In contrast to prior structural results, the geometry derived for the MgD_6 octahedron had a much more ideal configuration, with D−Mg−D angles ranging from 89.27(6) to 90.73(6)° and the octahedral-edge lengths from 2.7560(1)−2.7918(2) Å (300 K, see the Supporting Information for details). In the earlier room-temperature diffraction study,[10] Mg−D bonds are 1.957–1.979 Å, D−Mg−D angles were 74.5–105.7°, and the octahedral-edge lengths were 2.376–3.136 Å. The present Mg−D bond lengths compare much more favorably with those calculated by DFT structural optimization, which gave 1.961–1.964 Å for the Mg−D bond and 88.83–91.17° for D−Mg−D angles, etc.

The stability of crystal structure and bonding in $NaMgH_3$ can be discussed in terms of the tolerance factor, octahedral tilting, lattice distortion, and the MgH_6 octahedral distortion. As mentioned in the introduction, the geometrical stability of a perovskite structure and the compatibility of A−X and B−X bond lengths are generally evaluated by the tolerance

(24) Larson A. C., Von Dreele, R. B. *General Structure Analysis System*. LANL Report LAUR 86–748; Los Alamos National Laboratory: Los Alamos, NM, 1994.
(25) Lindstrom, R. M. *J. Res. Natl. Inst. Stand. Technol.* **1993**, *98*, 127–133.
(26) Udovic, T. J.; Neumann, D. A.; Lẽ.; ao, J.; Brown, C. M. *Nucl. Instrum. Methods Phys. Res. A* **2004**, *517*, 189.
(27) Baroni, S.; Dal Corso, A.; de Gironcoli, S.; Giannozzi, P. http://www.pwscf.org
(28) Kresse, G.; Furthmuller, J.; Hafner, J. *Europhys. Lett.* **1995**, *32*, 729.
(29) Yildirim, T. *Chem. Phys.* **2000**, *261*, 205.
(30) Bortz, M.; Bertheville, B.; Boettger, G.; Yvon, K. *J. Alloys Compd.* **1999**, *287*, 4–6.

Table 1. Rietveld Refinement Summary for $NaMgD_3$

chemical formula		$NaMgD_3$	
T (K)	5 K	300 K	370 K
radiation type		neutron	
diffractometer		HRPD (Cu(311) monochromator, $\lambda = 1.5403(2)$)	
measured 2θ range (°)		3–165	
cell setting, space group		orthorhombic, *Pnma* (No.62)	
a (Å)	5.43331(6)	5.44860(7)	5.4624(1)
b(Å)	7.64697(9)	7.6819(1)	7.7062(1)
c(Å)	5.36664(6)	5.39694(7)	5.41889(9)
V(Å^3)	222.976(5)	225.895(6)	228.107(8)
Z	4	4	
R_{F2}	0.0266	0.0271	0.0387
R_{wp}	0.0308	0.0310	0.0395
R_p	0.0258	0.0289	0.0334
χ^2	1.00	1.00	1.12
F_{NaMgD3} (wt %)	91.97(4)	92.32(5)	89.18(4)
no. of measd and obsd reflns	3101, 290	3101, 290	3101, 290
no. of constraints	No Constraints		
additional phase observed			
F_{MgO} (wt %)	5.21(1)	5.12(1)	7.94(1)
a (Å) *(Fm3̄m, No.225)*	4.2177(1)	4.2253(1)	4.2351(9)
F_{NaD} (wt %)	2.81(6)	2.55(6)	2.88(7)
a (Å) *(Fm3̄m, No.225)*	4.8355(2)	4.8714(3)	4.8961(4)

Table 2. Refined Structure Parameters in $NaMgD_3$

	this work					
	NPD experimental[a]			DFT calcd	ref 10	ref 21b
	5 K	300 K	370 K	0 K	NPD $NaMgD_3$	XRD $NaMgH_3$
Na (4*c*) *x*	0.0278(2)	0.0215(2)	0.0167(8)	0.0276	0.015(2)	0.0209(4)
y	0.25	0.25	0.25	0.25	0.25	0.25
z	−0.0052(4)	−0.0040(2)	−0.0032(8)	−0.0037	−0.018(2)	0.006(1)
U_{iso} [b]	0.0068(2)	0.0252(4)	0.0360(2)			
Mg (*4b*) *x*	0.0	0.0	0.0	0.0	0.0	0.0
y	0.0	0.0	0.0	0.0	0.0	0.0
z	0.5	0.5	0.5	0.5	0.5	0.5
U_{iso} [b]	0.0020(1)	0.0068(2)	0.0155(2)			
D1 (4*c*) *x*	−0.0220(2)	−0.0175(3)	−0.0139(5)	−0.0244	0.064(1)	0.003(7)
y	0.25	0.25	0.25	0.25	0.25	0.25
z	0.4218(2)	0.4273(3)	0.4308(4)	0.4202	0.483(1)	0.407(8)
U_{iso} [b]	0.0181(2)	0.0269(3)	0.0370(2)			
D2 (8*d*) *x*	0.2910(1)	0.2889(1)	0.2870(2)	0.2926	0.292(1)	0.304(6)
y	0.0401(1)	0.0374(1)	0.0345(1)	0.0413	0.040(1)	0.065(4)
z	0.7076(1)	0.7106(1)	0.7120(2)	0.7067	0.708(1)	0.761(8)
U_{iso} [b]	0.0173(1)	0.0265(2)	0.0346(6)			

[a] Refined occupancies of D1 and D2 are 0.985(7) and 0.975(5) at 5 K, 0.980(8) and 0.978(5) at 300 K, and 0.97(1) and 0.966(7) at 370 K, respectively. [b] Refined anisotropic thermal factors U_{ij} are as follows. 5 K: Na, $U_{11} = 0.0079(8)$, $U_{22} = 0.0056(8)$, $U_{33} = 0.0054(7)$, $U_{12} = 0$, $U_{13} = 0.0017(8)$, $U_{23} = 0$; Mg, $U_{11} = 0.0040(5)$, $U_{22} = 0.0023(6)$, $U_{33} = 0.0025(5)$, $U_{12} = 0.0004(4)$, $U_{13} = 0.0001(4)$; $U_{23} = -0.0014(7)$; D1, $U_{11} = 0.0226(6)$, $U_{22} = 0.0112(6)$, $U_{33} = 0.0209(6)$, $U_{12} = 0$, $U_{13} = 0.0016(4)$; $U_{23} = 0$; D2, $U_{11} = 0.0172(3)$, $U_{22} = 0.0200(3)$, $U_{33} = 0.0172(3)$, $U_{12} = -0.0015(3)$, $U_{13} = -0.0032(4)$, $U_{23} = 0.0012(3)$. 300 K: Na, $U_{11} = 0.025(1)$, $U_{22} = 0.022(1)$, $U_{33} = 0.022(1)$, $U_{12} = 0$, $U_{13} = -0.002(1)$; $U_{23} = 0$; Mg, $U_{11} = 0.0096(7)$, $U_{22} = 0.0087(9)$, $U_{33} = 0.0099(6)$, $U_{12} = 0.0007(6)$, $U_{13} = -0.0008(5)$, $U_{23} = 0.0001(9)$; D1, $U_{11} = 0.038(1)$, $U_{22} = 0.0163(9)$, $U_{33} = 0.0325(8)$, $U_{12} = 0$, $U_{13} = -0.0001(7)$, $U_{23} = 0$; D2, $U_{11} = 0.0252(4)$, $U_{22} = 0.0327(5)$, $U_{33} = 0.0254(4)$, $U_{12} = -0.0029(4)$, $U_{13} = -0.0081(5)$; $U_{23} = 0.0017(4)$. 370 K: Na, $U_{11} = 0.045(2)$, $U_{22} = 0.026(2)$, $U_{33} = 0.036(1)$, $U_{12} = 0$, $U_{13} = -0.0082(1)$, $U_{23} = 0$; Mg, $U_{11} = 0.015(1)$, $U_{22} = 0.014(1)$, $U_{33} = 0.0161(8)$, $U_{12} = 0.0020(8)$, $U_{13} = -0.0008(8)$; $U_{23} = -0.003(1)$; D1, $U_{11} = 0.050(1)$, $U_{22} = 0.016(1)$, $U_{33} = 0.045(1)$, $U_{12} = 0$, $U_{13} = -0.003(1)$, $U_{23} = 0$; D2, $U_{11} = 0.0308(6)$, $U_{22} = 0.0402(8)$, $U_{33} = 0.0326(6)$, $U_{12} = -0.0026(5)$, $U_{13} = -0.0124(7)$, $U_{23} = 0.0019(6)$.

factor (t). The symmetry will be lowered from the ideal cubic perovskite with space group *Pm-3m* when t deviates from unity. In the current case, the tolerance factor of $NaMgH_3$ is 0.931. The near-perfect regularity of the octahedra is incompatible with fixed rotation axes, and MgH_6 octahedra tilt in two directions: a primary rotation of φ around the b ($//[100]_c$) axis and a secondary tilt of Ψ about the c ($//[0\bar{1}1]_c$) axis, represented as $a^-b^+a^-$ according to Glazer's notation.[31] The MgH_6 octahedral tilting leads to the lattice distortion from the ideal cubic perovskite to a *Pnma* orthorhombic structure by $a_o = [0\ \bar{1}\ \bar{1}]a_c = \sqrt{2}a_c$, $b_o = [200]a_c = 2a_c$, $c_o = [0\ \bar{1}\ 1]a_c = \sqrt{2}a_c$ (subscript "o" represents the orthorhombic supercell and "c" is the cubic subcell). According to O'Keeffe and Hyde's early work,[32] the primary rotation angle φ in structures with *Pnma* symmetry can be deduced from the H positions and lattice parameters, by either $\varphi_1 = \tan^{-1}|-y(X_{(8f)})/\sqrt{48}|$, or $\varphi_2 = \cos^{-1}|\sqrt{2}c^2/(ab)|$, and the secondary tilt angle Ψ can then be derived from φ ($\psi = \tan^{-1}[\sqrt{2}(1 - \cos\varphi)/(2 + \cos\varphi)]$).[32] Upon tilting, the corner-sharing connectivity of MgH_6 octahedra is still maintained, shortening the Na−H distance. The first coordination sphere about the Mg cation remains unchanged. Only the soft Mg-H-Mg bond angles are disturbed, which

(31) The letters in Glazer's notation indicate the magnitude of the rotation about a give axis. Use of the letters *a*, *b*, and *c* implies unequal tilts about the x, y and z axes. A superscript is used to denote the phase of the octahedral tilting in neighboring layers. A positive superscript denotes the neighboring octahedral tilt in the same direction (in-phase) and a negative superscript indicates the tilt of neighboring octahedral in the opposite direction (out of phase). More details of Glazer's notation can be found in refs 32–34.

Table 3. Selected Atomic Distances (Å) and Bond angles (°) in $NaMgD_3$

	this work			ref 10
	5 K	300 K	370 K	300 K
Mg−D1 2×	1.9608(2)	1.9624(3)	1.9640(4)	1.979
Mg−D2 2×	1.9588(8)	1.9604(1)	1.9617(1)	1.957
Mg−D2 2×	1.9607(8)	1.9632(1)	1.9649(1)	1.971
mean Mg−D	1.9601	1.9620	1.9635	
Na−D1 1×	2.3084(2)	2.3378(3)	2.359(5)	2.472
Na−D1 1×	2.4863(2)	2.5454(3)	2.594(6)	2.714
Na−D1 1×	3.0209(2)	2.9660(3)	2.924(6)	2.725
Na−D1 1×	3.0861(2)	3.0762(3)	3.071(5)	3.006
Na−D2 2×	2.3262(1)	2.3486(2)	2.3685(3)	2.270
Na−D2 2×	2.6446(1)	2.6763(2)	2.705(4)	2.665
Na−D2 2×	2.6826(1)	2.6986(2)	2.7051(3)	2.754
Na−D2 2×	3.2366(1)	3.2005(2)	3.171(4)	3.257
mean Na−D	2.7235	2.7311	2.7373	
D1−D2 2×	2.7463(1)	2.7560(1)	2.7632(2)	2.376
D1−D2 2×	2.7495(1)	2.7598(1)	2.7720(2)	2.760
D1−D2 2×	2.7962(1)	2.7916(1)	2.7843(2)	2.795
D1−D2 2×	2.7965(1)	2.7918(2)	2.7884(2)	3.136
D2-D2 2 ×	2.75445(2)	2.7572(3)	2.7622(4)	2.770
D2−D2 2×	2.7885(4)	2.7915(5)	2.7908(6)	2.813
mean D−D	2.7719	2.7746	2.7768	
D1−Mg−D1	180	180	180	180
D1−Mg−D2 2×	91.04(5)	90.73(6)	90.52(1)	105.7
D1−Mg−D2 2×	90.96(5)	90.66(7)	90.25(9)	90.7
D1−Mg−D2 2×	88.96(5)	89.27(6)	89.48(1)	74.3
D1−Mg−D2 2×	89.04(5)	89.34(7)	89.75(9)	89.3
D2−Mg−D2 2×	90.705(11)	90.708(13)	90.59(1)	90.9
D2−Mg−D2 2×	180	180	180	180
D2−Mg−D2 2×	89.295(1)	89.292(1)	89.41(1)	89.1
Mg−D1−Mg	154.31(7)	156.27(9)	157.59(1)	159
Mg−D2−Mg	153.92(5)	155.53(6)	156.91(8)	153

can also be calculated from the rotation angle φ.[32] Figure 2 shows the MgH_6 octahedral tilting angle as a function of temperature. The octahedral tilting decreases with increasing temperature. Such a variation of octahedral tilting with temperature is consistent with the general observations in ABX_3 perovskites. Over a temperature range of 4−370 K, the dimensions of the $NaMgD_3$ perovskite ($a_o/\sqrt{2} \approx b_o/2 \approx c_o/\sqrt{2} \approx a_c$) are also close to each other, indicating a less-distorted lattice with increasing temperature.

As the temperature is increased, the mean Mg-D bond length was slightly elongated from 1.9601 Å (5 K) to 1.9635 Å (370 K), whereas the almost regular MgD_6 octahedra became even less distorted, as reflected by the D−Mg−D angles, i.e., 88.96(5)−91.04(5)° at 5 K, 89.27(6)−90.73(6)° at 300 K, and 89.48(1)−90.59(1)° at 370 K. The less deformed MgD_6 octahedra determined from the current refinement are reflected in the smaller discrepancy between the two octahedral rotation angle φ values (~4.3°, see the Supporting Information) compared to the earlier reported structure (~5.6°).[10] Octahedral distortion increases with increasing discrepancy between the two φ values. But even in the case of $LaFeO_3$, which exhibits a nearly 10° difference in φ values, the distortion is still not large, with only 1% deviation in the octahedron-edge lengths.[32] Thus, the large distortion of the MgD_6 octahedra in the previously reported $NaMgD_3$ structure[10] is not correct.

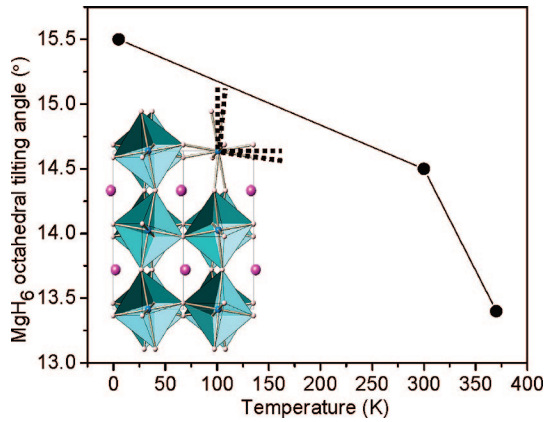

Figure 2. MgH_6 octahedra tilting angles (φ, $\varphi = \tan^{-1}|-y(X_{(8f)})/\sqrt{48}|$) of $NaMgH_3$ as a function of temperature. The refined structure at 300 K is presented in the inset. Large pink spheres are Na. Mg atoms (small blue spheres) are at the centers of the octahedra, and H atoms are located at the octahedral apexes. The broken lines indicate the MgH_6 octahedral tilting angles.

The stability of the MgH_6 octahedral distortion was also evaluated using bond valence methods.[33–35] The bond valence sums of Na and Mg cations calculated from the refined bond lengths agree very well with their formal valence (+1 and +2). Two hydrogen sites, D(4*c*) and D(8*f*), also exhibit similar bond valence sums with very small discrepancies from the formal valence of the hydrogen anion (−1), indicating the near-equal stability of these two hydrogen sites. Detailed information about bond valence calculations and results are provided in the Supporting Information. The bond valence calculation provides further evidence that the structure refined in the present paper better reflects the true crystal structure of $NaMgD_3$.

Finally, as mentioned earlier, a rapid H motion was observed in $NaMgH_3$, occurring only at elevated temperature.[22] We believe that such a motion can be rationalized from the details of the crystal structure. First, in perovskite oxide ionic conductors, oxygen ion conduction was found to be closely related to the anisotropic displacements of oxygen atoms and the mean O−O distances. [36] In $NaMgH_3$, the hydrogen at 5 K were localized and displayed a small thermal ellipsoid. With increasing temperature, the structure retained its *Pnma* symmetry, but the hydrogen ellipsoids are much larger than they were at 5 K and spread toward the neighboring hydrogen site. Figure 3 shows the views of the MgH_6 octahedra and the hydrogen thermal ellipsoids with temperature. The increased atomic displacements of the MgD_6 octahedra indicate the increased motion of the octahedra as a result of librations and dynamical disorder. Furthermore, the tilting of the octahedral framework plays an important role in determining the conductivity in the perovskite oxygen ion conductors. Many studies have shown that larger conductivities are generally observed in the structures with less octahedral tilt angles, [36–38] In $NaMgH_3$,

(32) O'Keeffe, M.; Hyde, B. G. *Acta Crystallogr., Sect. B* **1977**, *33*, 3802–3813.
(33) Brown, I. D. *Chem. Soc. Rev.* **1978**, *7*, 359–376.
(34) Bresem, N. E.; O'Keeffe, M. *Acta Crystallogr., Sect. B* **1991**, *47*, 192–197.
(35) Lufaso, M. W.; Woodward, P. M. *Acta Crystallogr., Sect. B* **2001**, *57*, 725–738.
(36) Kajitani, M.; Matsuda, M.; Hoshikawa, A.; Harjo, S.; Kamiyama, T.; Ishigaki, T.; Izumi, F.; Miyake, M. *Chem. Mater.* **2005**, *17*, 4235–4243.
(37) Hayashi, H.; Inaba, H.; Matsuyama, M.; Lan, N. G.; Dokiya, M.; Tagawa, H. *Solid State Ionics* **1999**, *122*, 1–15.
(38) Slater, P. R.; Irvine, J. T. S.; Ishihara, T.; Takita, Y. J. *Solid State Chem.* **1998**, *139*, 135.

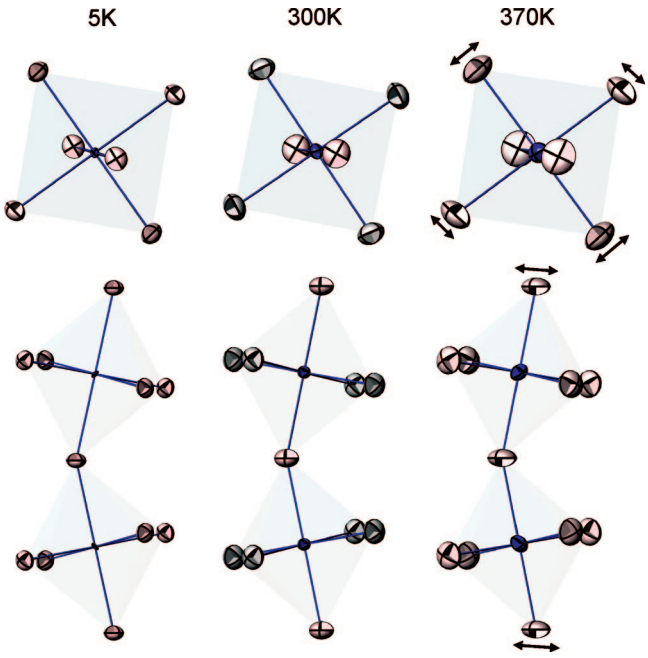

Figure 3. Top and side views of the atomic-displacement ellipsoids of H in the MgH_6 octahedra with temperature from 5 K (left) to 370 K (right). Mg atoms are at the centers of the octahedra with H atoms located at the octahedra apexes.

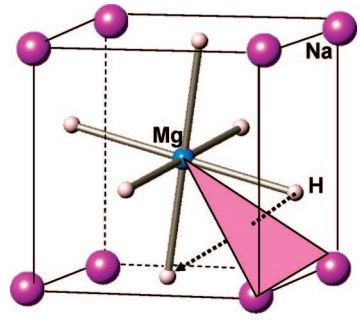

Figure 4. Schematic for the sublattice of $NaMgH_3$ with one H passing through the bottleneck defined by the triangle (2Na + 1Mg) to reach the adjacent vacant site.

the reduced MgH_6 octahedra tilt (Figure 2) with increasing temperature observed from NPD correlates with the temperature dependence of the hydrogen motion. In the ABX_3 perovskite structure, for ion X to move to the neighboring empty site, it must pass through the bottleneck defined by two A cations and one B cation[39,40] (the triangle shown in Figure 4). A more open bottleneck is generally associated with higher ionic conductivity. The bottleneck is most open if the structure is undistorted, with the X atom passing more easily through the normal to the triangle plane. If the octahedra are tilted, the direction of passage is displaced from the normal and the bottleneck triangle becomes more restricted. It is expected that the easiest migration of X atoms with the lowest activation energy would be observed for the smallest tilt angle. For an ionic conductor, the relation between conductivity (σ, i.e., transport property), activation energy (E_a) and the temperature generally follows the Arrhenius equation $\sigma T = \sigma_0 \exp(-E_a/kT)$, σ_0 is preexponential term, E_a is the activation energy for ion migration, k is the Boltzmann constant, and T is temperature in Kelvin.[41] The activation energy can be calculated from the slope of Arrhenius plots $\log \sigma(T) \approx (1000/T)$ or $\log(\sigma) \approx (1000/T)$. From the equation, without considering the structural variations and resultant changes in the activation energy, the diffusion rate of H atoms will increase as a function of temperature. But it is also obvious from the equation that the change in E_a has a dramatic effect on the ion migration beyond the effect of a rising temperature. Therefore, the impact of structural changes on the activation energy is a significant driver for the increased hydrogen migration rate observed in $NaMgH_3$ at high temperature. $NaMgH_3$ maintains a perovskite structure over the temperature range studied (up to 370 K), and we did not observe any structure variation such as a phase transition to a superionic phase with higher symmetry,[42] or any Na/Mg cation-site disordering. Therefore, the reduced tilt angle and lattice distortion with temperature is consistent with the observed increased hydrogen mobility in $NaMgH_3$ at high temperatures. Finally, we want to emphasize that the possible presence of X defects is necessary to detect the anion motions, and small amount of O vacancies are commonly observed in perovskite oxides synthesized at high temperatures.[43] Indeed, here in $NaMgH_3$ we also observed the presence of hydrogen vacancies (Table 2), which provide an essential condition for sensing such H motions. Further quasi-elastic neutron scattering experiments would provide more information of this high-H mobility at high temperature as found by NMR, and such experiments are currently underway.

2. Hydrogen Vibration and Lattice Dynamics. We have also probed the chemical environment and local bonding states of hydrogen in $NaMgH_3$ by NVS. The NVS data directly reflect the vibrational density of states and are particularly sensitive to the hydrogen vibrational displacements. Figure 5 shows the NV spectrum for $NaMgH_3$ collected at 4 K. The analogous deuteride spectrum (not shown) was similar to that of the hydride but downshifted in energy by roughly a factor of $1/\sqrt{2}$ because of the D/H mass ratio. With temperature increased to 370 K, the vibrational peaks smear out into broad bands and shift toward lower energy. Such variations of phonon bands with temperature are due to the anharmonicity (changes in bond lengths, bonding strengths and the lattice parameters) and increasing hydrogen displacements, consistent with the increased thermal ellipsoids observed in the high-temperature diffraction studies.

To better understand the spectrum, we performed first-principle phonon calculations. We started with the optimized $NaMgH_3$ structure mentioned above. The relaxed atomic positions agreed closely with our experimental values (Table 2). The phonon calculations were then performed with this optimized structure. A cell of $2a \times 1b \times 2c$ was used and the full dynamical matrix was obtained from a total of 24

(39) Cook, R. L.; Sammells, A. F. *Solid State Ionics* **1991**, *45*, 311.
(40) Sammells, A. F.; Cook, R. L.; White, J. H.; Osborne, J. J.; MacDuff, R. C. *Solid State Ionics.* **1992**, *52*, 111.
(41) Jiang, S. P.; Love, J. G.; Badwal, S. P. S. Key Engineering Materials. **1997**, *125–126*, 81–132.
(42) Perenthaler, E.; Schulz, H.; Beyeler, H. U. *Acta Crystallogr., Sect. B* **1981**, *37*, 1017–1023.
(43) Galasso, F., *Perovskites and High Tc Superconductors*; Routledge Press: New York, 1990; Chapter 2.

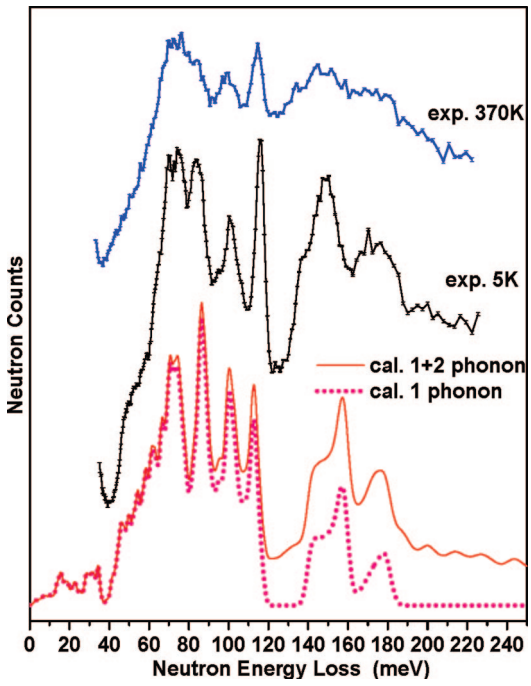

Figure 5. Neutron vibrational spectrum of $NaMgH_3$ at 5 and 370 K. Calculated spectra delineating both 1 phonon (dotted line) and 1 + 2 phonon (solid line) contributions are shown with the experimental data.

symmetry-independent atomic displacements (0.01 Å). The $NaMgH_3$ NV spectrum was computed for a 10 × 10 × 10 *q*-point grid within the incoherent approximation with instrumental resolution taken into account.[44] The primitive cell of $NaMgH_3$ contains 4 formula units (i.e., 20 atoms) giving rise to a total of 60 phonon branches.

NV intensities below 40 meV are attributed to translational lattice modes and metal-atom displacements and were not measured. The vibrational peaks above 40 meV are dominated by the vibrations of the MgH_6 octahedra. Phonon bands in the energy range of 40 to 80 meV are assigned to the Mg−H rocking modes, bands in the range of 80–120 meV are mainly the Mg−H bending modes, and bands above 120 meV are the Mg−H stretching modes. In each group of modes, H vibrations along Mg−-H2 bonds were found to have slightly higher energy than vibrations along Mg-H1 bonds, consistent with the refined Mg−H bond lengths (i.e., the Mg−H1 bond length is slightly longer than the mean Mg−H2 bond lengths). The calculated phonon modes for $NaMgH_3$ are in good agreement overall with the observed NV spectrum of $NaMgH_3$ (see Figure 5), again consistent with our refined structure. The spectroscopic calculations are also directly applicable to $NaMgD_3$.

3. Implications for Hydrogen Storage and Absorption Kinetics Modification. Magnesium hydride is a potentially important light-metal hydride for hydrogen-storage applications. Although it is more stable than desired, it has been investigated in great detail. Extensive studies have shown that the application of MgH_2 to hydrogen storage is limited by its sluggish absorption/desorption kinetics,[45,46] a result of its very low intrinsic diffusion coefficient.[47] Many efforts have been made to improve the hydrogen-storage properties of MgH_2. While most of the investigations have focused on overcoming the kinetic barriers via such strategies as mechanical activation,[45,46] particle size reduction, and defect introduction, no significant improvements have been achieved. On the other hand, additive elements such as Ni, Fe, Al, and Cu have also been used to modify the hydrogenation/dehydrogenation thermodynamics of MgH_2,[48] but only relatively weak effects have been observed. A more recent study found that the equilibrium pressure of a mixture of $2MgH_2$ + Si can be significantly increased compared to pure MgH_2, and alloying with Si can benefit the dehydrogenation process for pure MgH_2 by lowering the dehydrogenation enthalpy. However, the resultant dehydrogenated product Mg_2Si was difficult to rehydride after dehydrogenation because of kinetic limitations.[2] Effective modifications in hydrogenation/dehydrogenation thermodynamics have yet to be achieved.

The structure and recently observed rapid motion of hydrogen[22] make $NaMgH_3$ an interesting material for both storing hydrogen and facilitating kinetics modifications in related hydride systems. Pure $NaMgH_3$ has been shown to reversibly desorb/absorb hydrogen at 673 K.[21] Our study confirmed this reversible behavior and found that the hydriding/dehydriding reaction can actually proceed at temperatures as low as 623 K. Furthermore, previous isotherm results have shown that the heat of formation of $NaMgH_3$ is about −144 kJ/mol,[21] while those of MgH_2 and NaH are −76.15 and −56.44 kJ/mol,[49] respectively. This indicates that $NaMgH_3$ must be more stable than MgH_2. This difference in stabilities suggests a possible route for improving the hydrogenation properties of Mg_2Si via the alternative formation of $NaMgH_3$ instead of MgH_2.

Consistent with the previous study on the destabilization of MgH_2 with Si,[2] a milled mixture of MgH_2 + NaH + (3/2)Si started to desorb hydrogen at 523 K, a temperature lower than for pure MgH_2 and NaH. Heating up to 623 K, a complete desorption yielded a weight loss of 3.3 wt%. The XRD pattern (Figure 6) from a mixture dehydrogenated at 623 K showed a multiphase mixture of Mg_2Si, Si, Na, and a small amount of residual NaSi. By pressurizing this dehydrogenated mixture under 50 bar H_2 at 573 K, an uptake of 1.5 wt % hydrogen was achieved. The resulting XRD pattern (Figure 6) indicates the formation of $NaMgH_3$ and NaH as the hydride phases. Although the hydrogenation was not complete, it definitely shows that the addition of Na to Mg_2Si facilitated its partial hydrogenation through the formation of $NaMgH_3$. This suggests that proper doping of Mg_2Si with additional elements may render it more "hydridable."

In the present study, not only was the dehydrogenation enthalpy modified via the addition of Si, but the energy of

(44) Squires. G. L. *Introduction to the Theory of Thermal Neutron Scattering* Dover: New York, 1996).
(45) Huot, J.; Liang, G.; Schulz, R. *Appl. Phys. A: Mater. Sci. Process.* **2001**, *72*, 187.
(46) Bouaricha, S.; Dodelet, J. P.; Guay, D.; Huot, J.; Schulz, R. *J. Mater. Res.* **2001**, *16*, 2983.
(47) Bowman, R. C., Jr.; Fultz, B. *MRS Bull.* **2002**, *27*, 688.
(48) Zaluska, A. ; Zaluski, L.; Strom-Olsen, J. O. *Appl. Phys. A: Mater. Sci. Process.* **2001**, *72*, 157.
(49) Chase, M. W. NIST-JANAF Themochemical Tables, fouth edition in. *J. Phys. Chem. Ref. Data, Monograph 9* **1998**, 1.

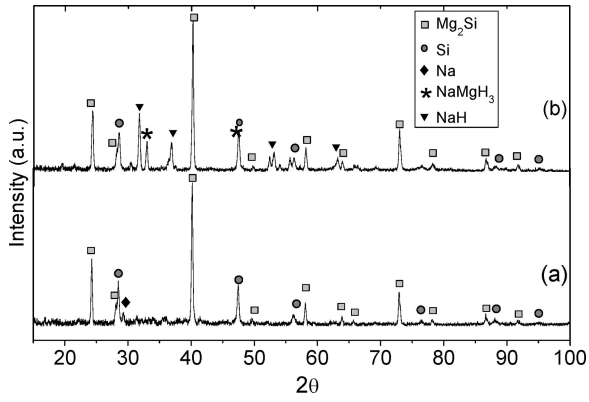

Figure 6. X-ray diffraction patterns from a NaH + MgH_2 + (3/2)Si mixture after dehydrogenation at 673 K and after rehydrogenation at 623 K under 50 bar H_2. After dehydrogenation, Mg_2Si is formed with Si and Na. After rehydrogenation, $NaMgH_3$ is formed with a small amount of NaH and Mg_2Si remaining. Symbols show locations of major peaks for Mg_2 Si (PDF 35–773), $NaMgH_3$, Si (PDF 27–1402), Na (PDF 22–948), and NaH (PDF 2–809), respectively.

the hydrogenation state was changed via the formation of $NaMgH_3$, which plays an indispensable role in the rehydrogenation process. Although the stable $NaMgH_3$ hydride forms during rehydrogenation, its stabilization energy is not as large as those of metal−Si alloys formed in the dehydrogenated state. Therefore, the effect does not completely cancel out, and there is still a large enough difference in stabilization energies to lower the dehydrogenation enthalpy. More importantly, there is a higher H mobility in $NaMgH_3$ because of its perovskite structure. Therefore, the hydrogenation rates are greatly improved compared to pure MgH_2.

Beyond $NaMgH_3$, the approach used to modify both thermodynamics and kinetics here can be applied generally. Other combinations of light elements with formation of stable hydride phases could thermodynamically promote the rehydrogenation process. Moreover, as discussed earlier, the more facile migration of H would likely be enhanced even more in a less distorted structure with smaller tilting angles. Therefore, and particularly for the perovskite structure, any approach that can adjust the tolerance factor to unity, such as by partially substituting the larger K cation for Na in $NaMgH_3$, could improve the hydrogen migration and thus accelerate the hydrogenation kinetics. In addition, as in the well-studied perovskite oxides,[36,37,50] a more effective approach to enhance the H mobility might be to increase the concentration of H vacancies by doping with small amounts of substituents that can exist as monovalent cations in place of the normally divalent *B*-type cations, e.g., doping with Li to form $Na(Mg_{1-x}Li_x)H_{3-x}$ and inducing x vacancies. Moreover, some nonstoichiometric compounds with a large concentration of structural anion vacancies, such as brownmillerites with a stoichiometry of $A_2B_2X_5$, usually exhibit dramatic ionic conductivity and could also be alternative candidates for designing and synthesizing new hydrides with attractive hydrogen-storage properties.

Conclusions

The crystal structure, lattice dynamics, and local metal−hydrogen bonding configuration of the perovskite hydride $NaMgH_3$ were systematically investigated using combined neutron powder diffraction, neutron vibrational spectroscopy, and first-principles calculations. $NaMgH_3$ crystallized in the orthorhombic $LaFeO_3$-type perovskite structure (*Pnma*) with $a^-b^+a^-$ octahedral tilting in the temperature range of 5 to 370 K. In contrast with previous structure studies, the refined Mg−H lengths and H−Mg-H angles indicated that the MgH_6 octahedra maintain a near ideal configuration, which is verified through the bond valence method and our DFT calculations, and is consistent with other perovskite oxides with similar tolerance factors. Resultant phonon calculations based on this structure were also consistent with the measured neutron vibrational spectrum. With increasing temperature, the lattice became less distorted, the MgH_6 octahedra tilting angles were reduced, and the H thermal ellipsoids became larger and spread toward the neighboring H, consistent with increased H mobility observed by NMR. The formation of $NaMgH_3$ played a key role in the rehydrogenation of normally "inert" Mg_2Si, via the addition of NaH. In this way, Mg can be partially hydrogenated through the formation of $NaMgH_3$, presumably aided by the much higher H mobility in the latter. The stability and high hydrogen mobility in $NaMgH_3$ are representative of the intriguing structural chemistry in perovskite-type and other related hydrides, which may open up new directions to modify and design new alloy hydrides with desirable storage properties.

Acknowledgment. This work was partially supported by the DOE through EERE Grant DE-AI-01-05EE11104 (T.J.U.), and BES Grant DE-FG02-98ER45701 (T.Y.).

Supporting Information Available: Detailed information concerning octahedral tilting angles with temperatures, comparisons of octahedral tilting and distortion with prior reported structures and some $GdFeO_3$-type perovskite oxides, bond valence calculations, and neutron diffraction patterns at 5 and 370 K (PDF). This material is available free of charge via the Internet at http://pubs.acs.org.

(50) Wu, H.; Davies, P. K. *J. Am. Ceram. Soc.* **2006**, *89* (6), 2250–2263.

CM703356V